Yrast structures in the neutron-rich isotopes ^{59,60}Fe and the role of the $g_{9/2}$ orbital

A. N. Deacon,[1,*] S. J. Freeman,[1] R. V. F. Janssens,[2] M. Honma,[3] M. P. Carpenter,[2] P. Chowdhury,[4] T. Lauritsen,[2] C. J. Lister,[2] D. Seweryniak,[2] J. F. Smith,[1,†] S. L. Tabor,[5] B. J. Varley,[1] F. R. Xu,[6] and S. Zhu[2]

[1]*Schuster Laboratory, University of Manchester, Manchester M13 9PL, United Kingdom*

[2]*Argonne National Laboratory, Argonne, Illinois 60439, USA*

[3]*Center for Mathematical Sciences, University of Aizu, Tsuruga, Ikki-machi, Aizu-Wakamatsu, Fukushima 965-8580, Japan*

[4]*University of Massachusetts, Lowell, Massachusetts 01854, USA*

[5]*Department of Physics, Florida State University, Tallahasse, Florida 32306, USA*

[6]*Department of Technical Physics, Peking University, Beijing 100871, People's Republic of China*

(Received 9 August 2007; published 2 November 2007)

The structure of the neutron-rich isotopes ^{59,60}Fe has been studied with the Gammasphere detector array using fusion-evaporation reactions. Level schemes for these nuclei are presented which have been extended to spins of $\sim 20\hbar$. Both isotopes exhibit regular, near-yrast γ-decay sequences which are generated by the intrusion of the $g_{9/2}$ orbital into the fp shell-model space. Lower-spin, natural-parity levels are discussed within the context of shell-model calculations using the GXPF1A interaction in the full fp model space. Experimental features of the high-spin bands are compared with total Routhian surface calculations.

DOI: 10.1103/PhysRevC.76.054303 PACS number(s): 21.60.Cs, 23.20.En, 23.20.Lv, 27.50.+e

I. INTRODUCTION

Neutron-rich fp-shell nuclei have been the subject of much recent investigation. Primarily, such work has been motivated by increasing evidence for unexpected modifications of the single-particle structures of these exotic systems due to aspects of the nucleon-nucleon interaction not immediately apparent in near-stable systems. In understanding these developments, a great deal of synergistic effort is occurring on both the theoretical and experimental fronts. One such example is the development of the GXPF1 effective interaction [1], which led to predictions of subshell gaps at $N = 32$ and 34. These new gaps in the single-particle levels are attributed to an attractive $\pi f_{7/2} - \nu f_{5/2}$ monopole interaction, which is weakened as protons are removed from the $\pi f_{7/2}$ orbital. Combined with the large spin-orbit splitting between the $2p_{3/2}$ and $2p_{1/2}$ orbitals, this results in a large energy gap at $N = 32$ for $20 \leqslant Z \leqslant 24$, which is filled at higher Z as the $\nu f_{5/2}$ orbital is pushed down between the two $2p$ orbitals. The $N = 32$ gap, and its demise with increasing Z, has been verified by measurements of energy levels in Ti, Cr, and Fe isotopes [2–6] and by recent data on ^{52}Ca [7]. In the latter case, a two-proton knockout reaction was used to populate only the ground state and a 3^- level at an excitation energy of $\sim$4 MeV. Whereas this 3^- state is understood as the promotion of protons across the $Z = 20$ shell closure, the 2_1^+ state at 2.6 MeV, *not* directly fed in this knockout reaction, is a neutron particle-hole excitation across the $N = 32$ gap.

The predictions of changing structure in the fp shell and, in particular, the appearance of new subshell gaps at large neutron excess, are being systematically tested by a number of experimental measurements. Recent data on the $B(E2; 0^+ \rightarrow 2^+)$ transition rates in the even-even isotopes ^{52,54,56}Ti [3] have confirmed the existence of a gap at $N = 32$, but not at $N = 34$. This led to the development of the modified GXPF1A interaction [8], where five $T = 1$ matrix elements of the interaction have been readjusted. These matrix elements mainly involve the $\nu p_{1/2}$ and $\nu f_{5/2}$ single-particle orbitals, resulting in a satisfactory description of all the known experimental levels in the odd and even Ti nuclei [2,9].

Further information on single-particle structures in neutron-rich fp-shell nuclei has been gained recently via knockout reactions, such as ^{9}Be(^{57}Cr,^{56}Cr+γ)X [10]. The calculation of spectroscopic factors using the GXPF1A interaction in the full fp model space leads to predictions of spin-parities consistent with previous experimental assignments [5,11,12].

Detailed experimental studies of neutron-rich Cr isotopes have been carried out using a variety of populating reactions [12–14]. Comparison of the energy systematics of the first-excited 2^+ states in the even-even isotopes illustrates the existence of the subshell gap at $N = 32$, albeit not as large as in the Ti isotopes [15]. Evidence for a gap at $N = 34$ is notably absent once more, and the 2_1^+ energies decrease steadily from 1006 keV in ^{56}Cr$_{32}$, through 880 keV (^{58}Cr$_{34}$) and 645 keV (^{60}Cr$_{36}$) to 446 keV in ^{62}Cr$_{38}$. This fall in excitation energy has been the subject of various interpretations; in the most detailed experimental studies, which include the energy of the first 4^+ states in the form of the ratio $R(4^+/2^+)$, the low-lying energy systematics of the neutron-rich Cr isotopes have been discussed in terms of a softening of nuclear shape with increasing neutron number [14]. This is in contrast with the suggestion of a strong deformation proposed in Ref. [15].

Studies of the neutron-rich Cr isotopes have also extended to high spin, where structures involving excitations clearly beyond the fp model space have been observed. These structures involve the intruder $\nu g_{9/2}$ orbital, which appears to have an increasing influence on collective features of nuclear

*alick.deacon@manchester.ac.uk

†Current address: School of Engineering and Science, University of Paisley, Paisley PA1 2BE, UK.

structure, due to its potential for deformation-driving effects and a rather small energy gap between the fp and $g_{9/2}$ orbitals. Indeed, regular decoupled bands of stretched-$E2$ transitions in ^{55,57}Cr [12,16] are indicative of the prolate deformation induced by the excitation of the odd neutron in these systems to the $1/2^+[440]$ orbital of $g_{9/2}$ spherical parentage. In contrast, in ^{59}Cr an isomeric $9/2^+$ state at 503 keV suggests a $9/2^+[404]$ configuration, consistent with an odd $g_{9/2}$ neutron driving a spherical or mildly oblate core toward more pronounced oblate deformation [13]. This sudden change in the structure of the odd-A neutron-rich Cr isotopes, driven by the appearance of the $g_{9/2}$ orbital at low energies, is also reflected in the shell-model calculations for both odd-A and even-even isotopes. For $N \leqslant 34$, calculations employing the GXPF1A interaction in the full fp model space reproduce reasonably well the low-lying natural-parity states, to within 100 keV in many cases [14]. However, for ^{59,60}Cr the measured energy levels exhibit an overall compression with respect to the results of these calculations. This indicates, again, the influence of the $g_{9/2}$ orbital at low excitation energy in neutron-rich Cr nuclei.

The Fe isotopes, with $Z = 26$, represent the next logical step in the investigation of neutron-rich fp-shell nuclei. Recent data from deep-inelastic collisions have provided the first extensive information on ^{64}Fe [17]. A notable gap in the detailed knowledge of nuclear structure now exists between this isotope and ^{58}Fe, an issue that is partially addressed here. For $Z = 26$, the predictions of the GXPF1A interaction are that the $\nu f_{5/2}$ orbital will have been pushed below the $\nu p_{1/2}$ state as a result of the increasing attractive strength of the monopole interaction described above, thus closing the $N = 32$ subshell gap altogether [8]. A consistent approach to nuclear structure in the region would suggest that the $g_{9/2}$ orbital should drive toward collectivity in the Fe isotopes as well. In particular, high-spin yrast bands should be identifiable with excitations involving this orbital. In addition, detailed studies of lower-spin states provide a test of fp-shell calculations over a wider range of systems.

Populating yrast states in very neutron-rich fp-shell nuclei is a nontrivial task. As the region is below that obtainable via fission-fragment spectroscopy, one must rely on deep-inelastic or heavy-ion-induced fusion-evaporation processes. It has been shown that deep-inelastic collisions at beam energies 15%–20% above the Coulomb barrier can be used to populate relatively high angular-momentum states in many isotopes in the region [18–20]. However, these methods are often complicated by the need to employ cross-coincidence techniques between binary reaction products in order to identify the isotopes to which detected γ rays correspond. This method can be made impossible when reaction products undergo fission, and so isotopic identification then relies on the existence of previously known transitions. The alternative of identifying and measuring coincident ejectile ions (as, for example, in Ref. [21]), while providing isotopic assignments, suffers from a lack of statistics, which is associated with the finite entrance solid angle of the available magnetic spectrometers. The construction of level schemes using $\gamma\gamma$ coincidence techniques is then difficult.

The method employed in the present work uses heavy-ion-induced fusion-evaporation reactions, operated under inverse kinematics, to bypass these problems. As the reaction recoils have high linear momentum, isotopic selection may be achieved through the use of a recoil-mass spectrometer and its focal-plane detector. Though fusion-evaporation is commonly associated with the production of proton-rich nuclei, the combination of a ^{48}Ca projectile, with its large neutron excess, and neutron-rich, long-lived radioactive targets such as ^{14}C, can provide access to the neutron-rich fp-shell nuclei, especially if charged-particle evaporation channels can be studied [13].

In the current work, high-spin states in ^{59,60}Fe have been populated. The yrast and near-yrast structures are compared with the results of shell-model calculations using the GXPF1A interaction in the full fp model space, and the role of the $g_{9/2}$ orbital in the experimental data is assessed by comparison with total Routhian surface calculations.

II. EXPERIMENTS

Data were obtained through two separate experiments performed at Argonne National Laboratory. In each experiment, a beam of $^{48}Ca^{11+}$ ions at 2.75 MeV/nucleon was delivered by the Argonne Tandem Linear Accelerator System (ATLAS) and used to bombard an isotopically enriched carbon target of approximate thickness 100 μg/cm^2. Targets of ^{13}C and ^{14}C were used in two separate experiments. The enrichment of each target was approximately 90%, the main contaminant being ^{12}C. Guided by excitation functions from Ref. [6], the beam energy was chosen to optimize production of two-particle evaporation channels. Prompt electromagnetic radiation was detected at the target by the Gammasphere detector array [22], consisting of 91 and 100 Compton-suppressed high-purity Ge detectors in the two experiments. Recoiling ions from the target were dispersed according to their mass-to-charge ratio, A/q, using the Fragment Mass Analyzer (FMA) [23], and their energy-loss characteristics were determined by a segmented-anode ion chamber behind the focal plane. The FMA was tuned to deliver ions of $A/q = 59/17$ to the center of the focal plane in the first experiment, and $A/q = 60/17$ in the second. Data acquisition was triggered by the detection of one or more γ rays in coincidence with the arrival of a recoil ion in the focal plane detector, which in both experiments was a parallel-grid avalanche counter (PGAC). Beam currents of around 5 pnA resulted in a total of 1×10^8 and 3×10^8 recoil-γ events being written to magnetic tape over periods of 58 and 128 h in the two experiments.

The occurrence of charge-state ambiguities between recoils of different A means the measured PGAC positions (proportional to A/q) are often insufficient to resolve events corresponding to recoils of different A (for example, $A/q = 57/16 = 3.56$ and $A/q = 60/17 = 3.53$). The time-of-flight measurements through the FMA (T) can be combined with the energy loss of recoils in the ion chamber (E) to form the parameter ET^2, which is proportional to the mass of the recoils. Thus, a plot of ET^2 against A/q can be used to separate recoils according to different mass groups. Selection by atomic number may be achieved by placing polygonal gates on a plot of the energy loss of recoils in the first two segments of the

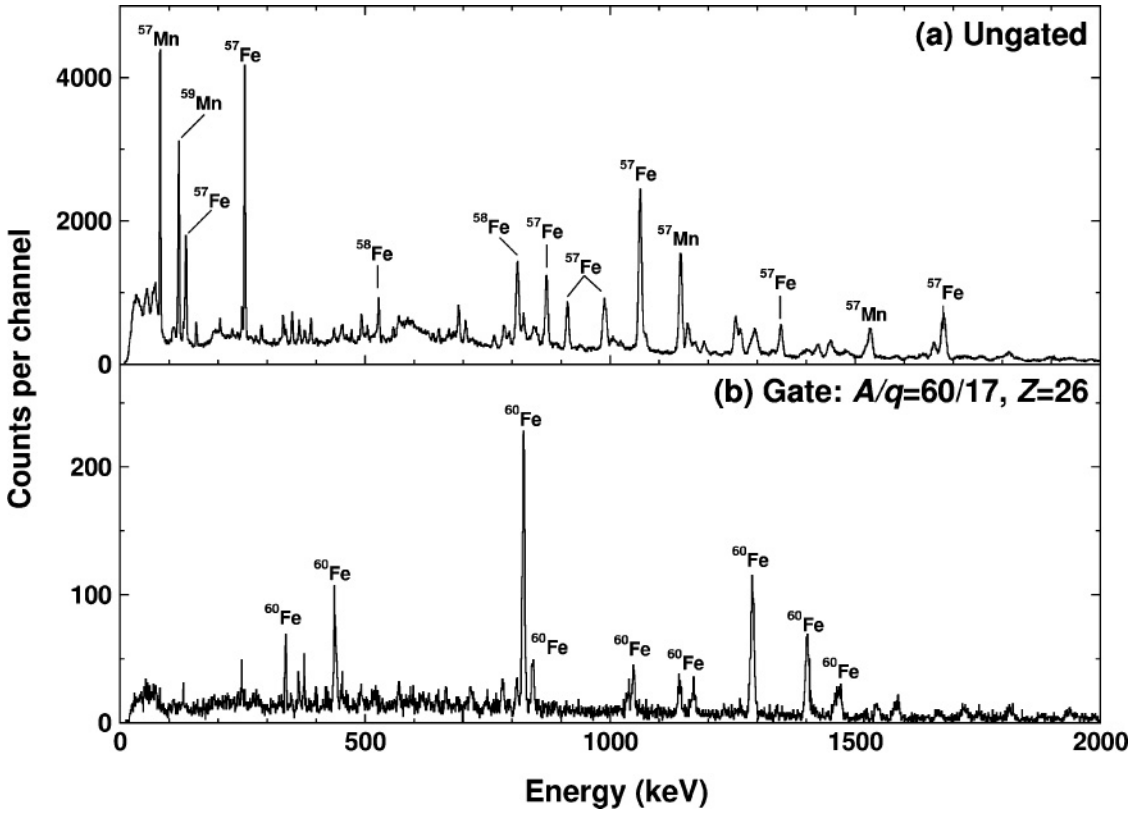

FIG. 1. γ-ray singles spectra under various conditions: (a) ungated spectrum; (b) spectrum gated by $A/q = 60/17$ and $Z = 26$. Peaks are labeled by their isotopic assignment.

ion chamber, ΔE, against the total energy loss E. Examples of both these plots for the two experiments may be found in Fig. 1 of Ref. [13] and Fig. 1 of Ref. [12].

Fe recoils resulted from neutron-evaporation channels (xn) and were consequently the most strongly populated, with cross sections estimated to be of the order of 100 mb for the $3n$ and $4n$ channels, and millibarn cross sections for the $2n$ channel [24]. A polygonal software gate placed around the Fe group in the plot of E vs ΔE served to reduce the background and cut down contributions from scattered beam, whereas a similar software gate around the relevant mass group in the plot of ET^2 vs A/q reduced the level of contamination from other Fe isotopes. Figures 1(a) and 1(b) provide example spectra to demonstrate the effectiveness of applying such mass and Z gates. The peak-to-total ratio for the 824-keV $2_1^+ \rightarrow 0_1^+$ transition in ^{60}Fe increases from 0.3% in the ungated spectrum, to 4.8% in the spectrum formed from both the mass and Z gates applied simultaneously.

Level schemes of ^{59,60}Fe were constructed using recoil-gated $\gamma\gamma$ coincidence matrices and conventional coincidence analysis techniques. Angular distribution analysis provided the means for deducing spin-parity assignments to excited states. The measured angular distributions $W(\theta)$ were fitted with the formula

$$W(\theta) = A_0[1 + a_2 P_2(\cos\theta) + a_4 P_4(\cos\theta)], \qquad (1)$$

where $P_L(\cos\theta)$ are Legendre polynomials. Where no statistically significant a_4 coefficient could be extracted, a fit of the form $W(\theta) = A_0[1 + a_2 P_2(\cos\theta)]$ was made from which the a_2 coefficients were deduced.

III. RESULTS

A. ^{59}Fe

The level scheme for ^{59}Fe deduced in the current work consists of two main regular decay pathways feeding somewhat irregular low-lying states with some weaker side structures. It is given in Fig. 2. The energies of levels in this scheme are listed in Table I, along with their spin-parity assignments and the properties of the γ-ray transitions between them. The a_2 and a_4 coefficients given in Table I were deduced from the fits to the γ-ray angular distributions, representative examples of which are plotted in Fig. 3.

The ground-state spin-parity of ^{59}Fe has been assigned as $3/2^-$ [25]. A previous study of ^{59}Fe [26] using a fusion-evaporation reaction identified seven excited states with energies of 472.7, 570.8, 1023.1, 1517.2, 2312.2, 3559.6, and 3737.7 keV, connected by nine γ-ray transitions with energies 472.7, 570.8, 1023.1, 550.4, 452.3, 494.1, 795.0, 1247.4, and 1425.5 keV. The level scheme deduced in the current work confirms the placement of all these transitions and levels, along with their spin-parity assignments, which form a subset of those discussed here. In addition, transitions of 1391.5 and 1790 keV, which were previously observed but not placed [26], have now been included in the level scheme of ^{59}Fe. The

TABLE I. Energies (in keV), spins and parities of excited states in ^{59}Fe. Measured transition energies E_γ and relative intensities I_γ (corrected for efficiency and internal conversion) of deexciting γ rays are listed. The angular distribution coefficients, a_2 and a_4, are also given where known. The a_2 and a_4 coefficients marked with superscripts were derived from the angular distribution of the area of an unresolved doublet near an energy of ∼2053 keV.

Level energy	J^π	E_γ (keV)	I_γ	a_2	a_4
473.0(1)	$5/2^-$	473.0(1)	21.5(4)	−0.16(3)	
570.3(1)	$5/2^-$	570.4(1)	56.8(4)	−0.35(2)	
1022.6(1)	$7/2^-$	452.4(1)	55.3(19)	−0.34(2)	
		549.5(1)	3.34(23)	−0.38(11)	
		1022.6(1)	70(3)	+0.20(3)	−0.15(4)
1516.7(1)	$9/2^+$	494.1(1)	100(3)	−0.24(1)	
1599.1(1)	$9/2^-$	1029.1(21)	0.67(22)		
		1126.2(1)	15.7(8)	+0.29(7)	−0.18(10)
1936.5(16)		1366.2(13)	1.5(4)		
2311.8(1)	$13/2^+$	795.0(1)	83(3)	+0.37(3)	−0.08(3)
2414.8(2)	$11/2^-$	815.7(3)	2.43(21)	+0.88(10)	−0.24(20)
		1391.9(2)	16.7(10)	+0.31(7)	−0.09(8)
2483.5(2)	$13/2^+$	966.7(2)	7.5(5)	+0.33(9)	−0.19(11)
3051.6(3)	(13/2, 15/2)	568.0(3)	1.7(3)		
3179.4(2)	$13/2^-$	1580.7(3)	6.9(5)	+0.37(13)	−0.22(18)
3429.5(2)	$15/2^-$	250.1(1)	4.51(21)	−0.28(5)	
		1014.6(1)	15.0(7)	+0.10(7)	−0.19(9)
3558.4(2)	$15/2^+$	1246.7(1)	18.2(8)		
3738.6(1)	$17/2^+$	1426.4(1)	57.0(19)	+0.36(8)	−0.15(12)
4141.6(7)		962.3(5)	1.59(24)		
4272.8(3)	$17/2^+$	714.8(4)	1.44(18)	−0.47(15)	
		1221.0(5)	1.84(21)	+0.69(41)	
		1788.7(6)	3.9(4)	+0.37(13)	−0.22(18)
4329.5(13)		2017.7(11)	2.7(4)		
4870.3(4)	$19/2^-$	1440.8(3)	8.3(5)	+0.44(7)	−0.18(9)
4978.0(3)	$(19/2^+)$	1240.2(8)	2.0(3)		
		1419.6(2)	10.0(6)		
5542.4(2)	$21/2^+$	1270.2(14)	0.9(3)		
		1804.3(1)	24.7(10)	+0.45(6)	−0.21(8)
5895(3)		1565.6(21)	1.0(3)		
6023.7(12)		2285.6(10)	3.2(4)		
6923.6(4)	$23/2^-$	2053.3(1)	8.2(6)	+0.38(7)[a]	
7030.2(3)	$(23/2^+)$	2052.2(1)	6.5(5)	+0.38(7)[a]	
7233.1(9)		1690.7(7)	2.9(3)		
7671.2(5)	$(25/2^+)$	2128.8(4)	9.1(5)		
7764.2(16)		2221.8(13)	2.3(4)		
7928.6(5)	$27/2^-$	1005.0(2)	5.0(3)	+0.25(13)	
8552.6(15)		1319.5(11)	1.11(24)		
9544.6(18)	$(27/2^-)$	2514.3(15)	2.6(4)		
10025.7(9)	$(31/2^-)$	2097.1(7)	4.6(4)		
10203.1(16)	$(29/2^+)$	2531.8(13)	3.1(4)		
12636(3)	$(35/2^-)$	2611(3)	1.9(5)		
12915.0(24)	$(33/2^+)$	2711.9(15)	2.9(4)		
14352(4)	$(39/2^-)$	1715.6(22)	0.9(3)		

current work yields significant extensions of the previous level scheme, pushing decay sequences to spins approaching $20\hbar$, with new decay pathways revealed by improved detection sensitivity.

The negative-parity states, placed on the left-hand side of Fig. 2, are mainly formed from a sequence of $E2$ transitions feeding the low-lying states. The associated transition energies exhibit some regularities which will be discussed later. Coincidence relationships in this sequence were established from gated γ-ray spectra, a representative example of which is shown in Fig. 4(a). The positive-parity states are grouped to the right in Fig. 2 and are composed of one regular main sequence extending to spin 33/2, and a weaker, but still regular, side band populated to $27/2\hbar$. Representative spectra illustrating these bands are in Figs. 4(b) and 4(c). These bands are also fed in numerous places by weak and irregular transitions.

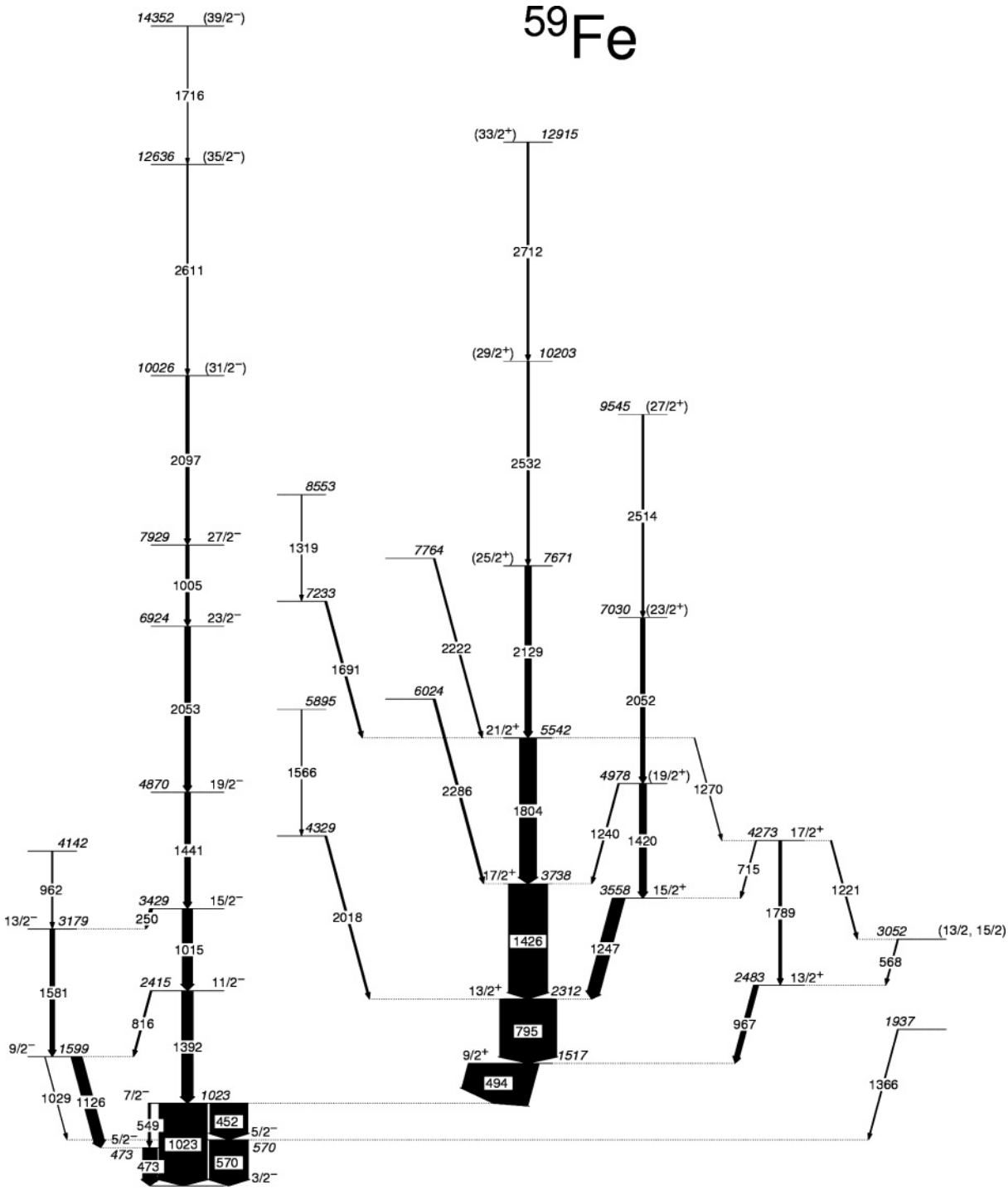

FIG. 2. Level scheme of ^{59}Fe deduced in the current work. The levels are labeled by their spin-parity and excitation energy to the nearest keV. The widths of the arrows indicate the relative intensities of the γ-ray transitions, normalized to the ground-state feeding.

The 494-keV transition appears to be self-coincident, but the second transition is difficult to place in the current level scheme. Transitions with energies of 891, 1750, and 2113 keV are clearly associated with this second 494-keV transition, with the possibility of a second 1392-keV transition, but none of these could be placed from the available data. Other doublets in the γ-ray spectra, such as the peak at 570 keV, which appears self-coincident in the $\gamma\gamma$ matrix, have led to more successful transition placements. Gates set at 1392 and 1221 keV point to a shift in the centroid of this peak in the spectrum and have led to the placement of the 568-keV transition feeding the $13/2^+$ state at 2483 keV.

The 1392-, 1015-, 1441- and 1005-keV transitions all have angular distributions indicative of a stretched-quadrupole nature (positive a_2 and negative a_4 coefficients). The angular distribution for the total sum of the doublet formed by the

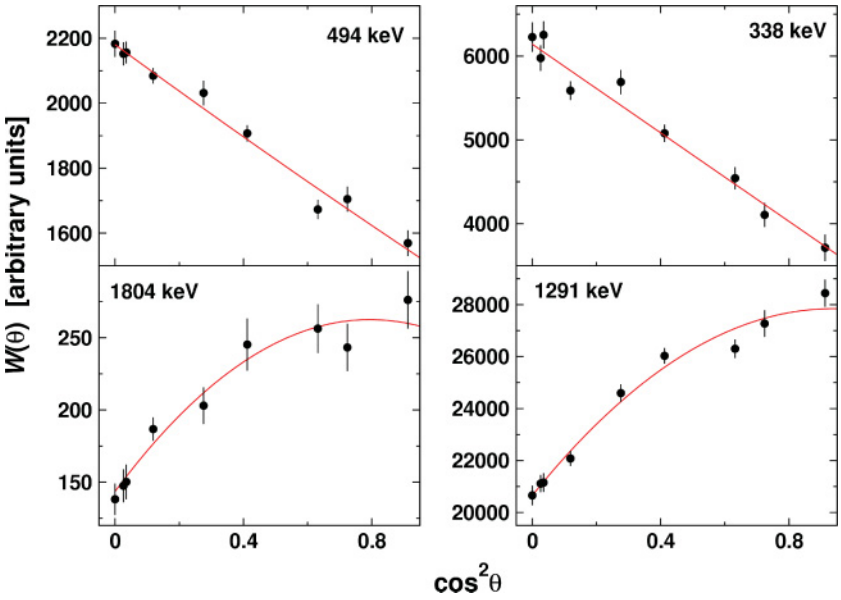

FIG. 3. (Color online) Representative angular distributions for transitions in ^{59}Fe (left panel) and ^{60}Fe (right panel), labeled by energy in keV. The lines represent least-squares fits of the form given in Eq. (1), from which the a_2 and a_4 given in Tables I and II were deduced (see text for details).

2052- and 2053-keV transitions also has a positive a_2 coefficient, although no statistically significant a_4 coefficient could be deduced; both are taken to have a stretched-quadrupole character. This leads to the assignment of spin-parities $11/2^-$, $15/2^-$, $19/2^-$, $23/2^-$, and $27/2^-$ to the states at 2415, 3429, 4870, 6924, and 7929 keV. The 2097-, 2611-, and 1716-keV transitions are assumed to continue this sequence of stretched-quadrupole transitions, leading to the tentative assignments of $J^\pi = 31/2^-, 33/2^-$ and $35/2^-$ to the levels at 10026, 12636, and 14352 keV, respectively. It should be noted that the 1005-, 1015-, and 1023-keV transitions form a triplet of peaks in the γ-ray spectra, and their angular distributions were determined by simultaneously fitting all three components of this triplet. Difficulties in this procedure may account

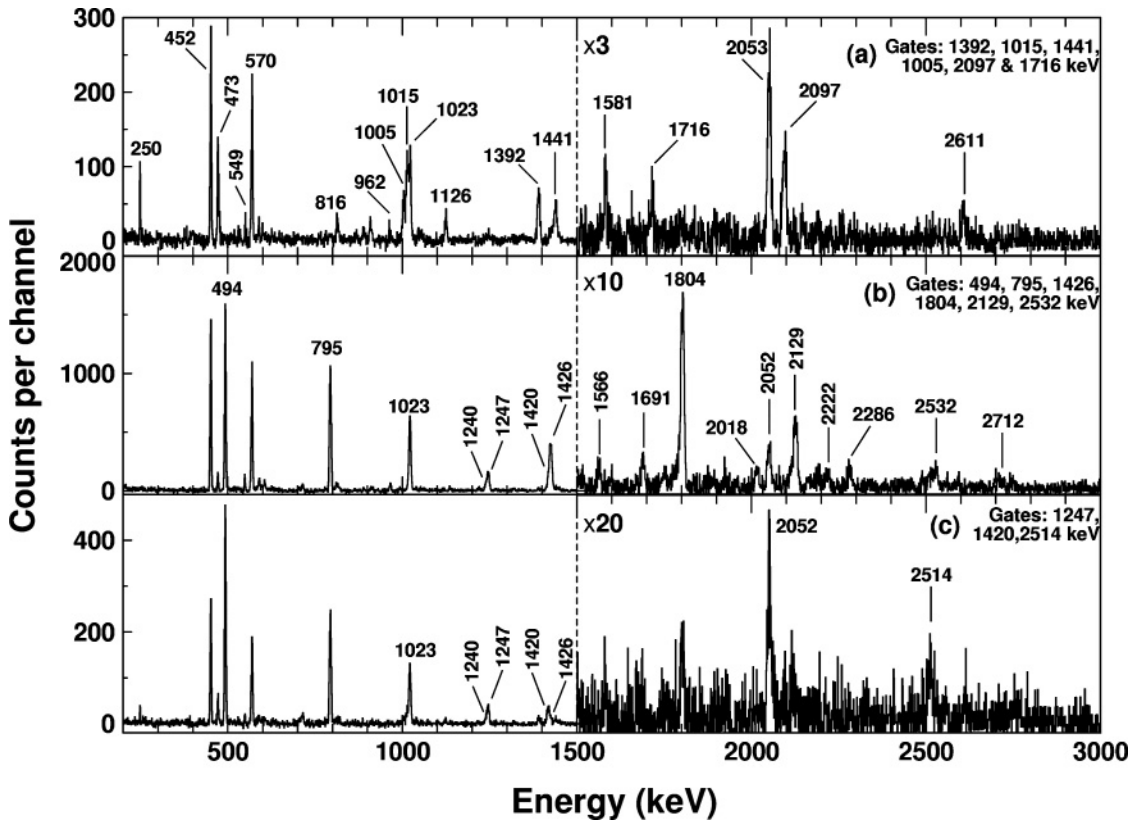

FIG. 4. Representative coincidence γ-ray spectra gated by transitions in ^{59}Fe. Peaks are labeled by energy in keV. Note the change in vertical scale at 1500 keV by the factors indicated in each panel.

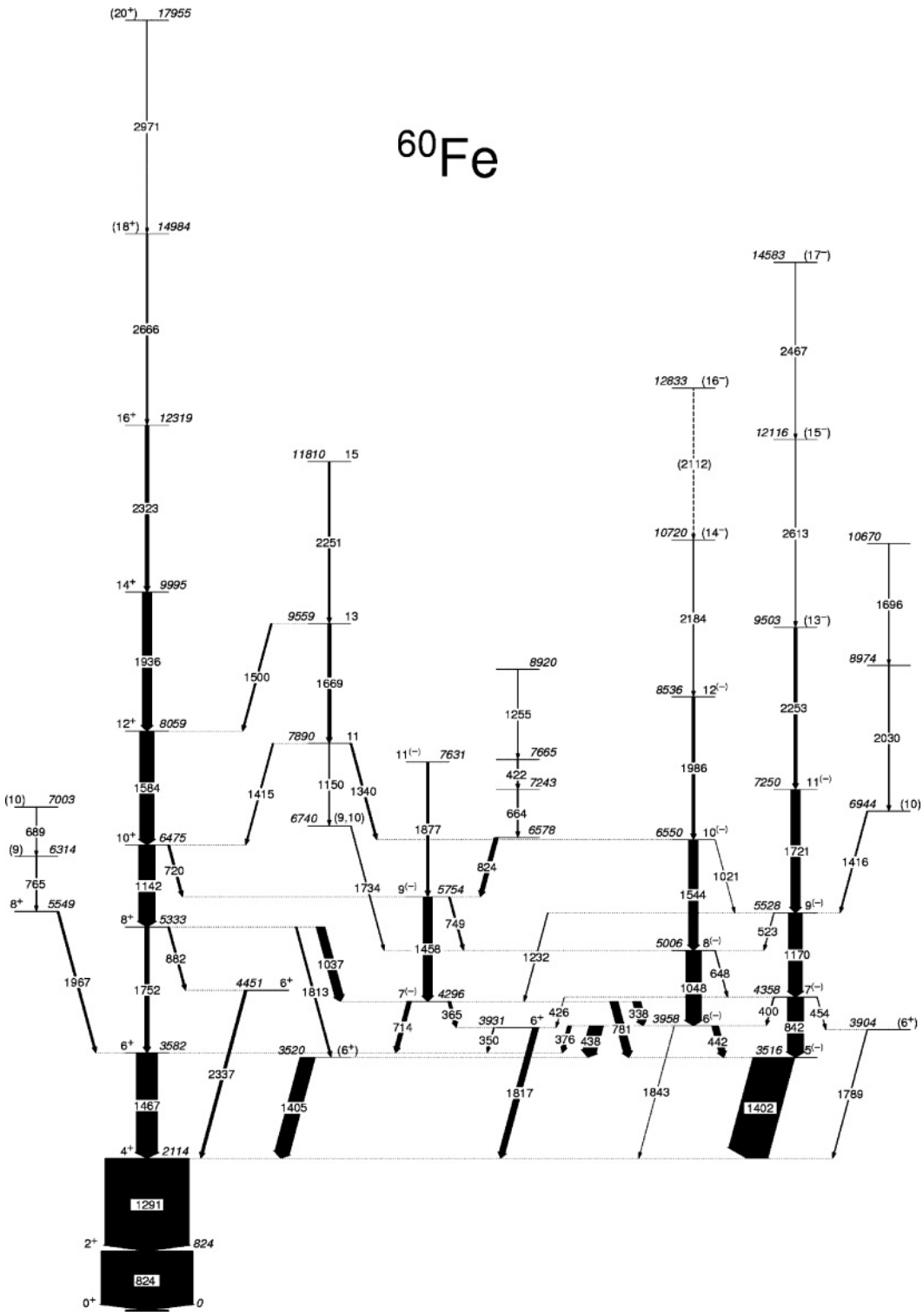

FIG. 5. Level scheme of ^{60}Fe deduced in the current work. The levels are labeled by their spin-parity and excitation energy to the nearest keV. The widths of the arrows indicate the relative intensities of the γ-ray transitions, normalized to ground-state feeding.

for the fact that the anisotropy of the 1015-keV transition appears to be significantly less than would be expected for a stretched-$E2$ transition at this spin range (the values of a_2 and a_4 for a stretched $15/2 \rightarrow 11/2$ transition, in the case of full alignment, are $+0.43$ and -0.20, respectively). It is also worth noting that this angular distribution may be affected by the presence of the 1014.5-keV line in ^{27}Al that is present in Ge spectra because of (n, n') reactions on the Al cap of the detectors [27]. However, the $15/2^-$ assignment to the state at 3429 keV is supported by following the parallel decay

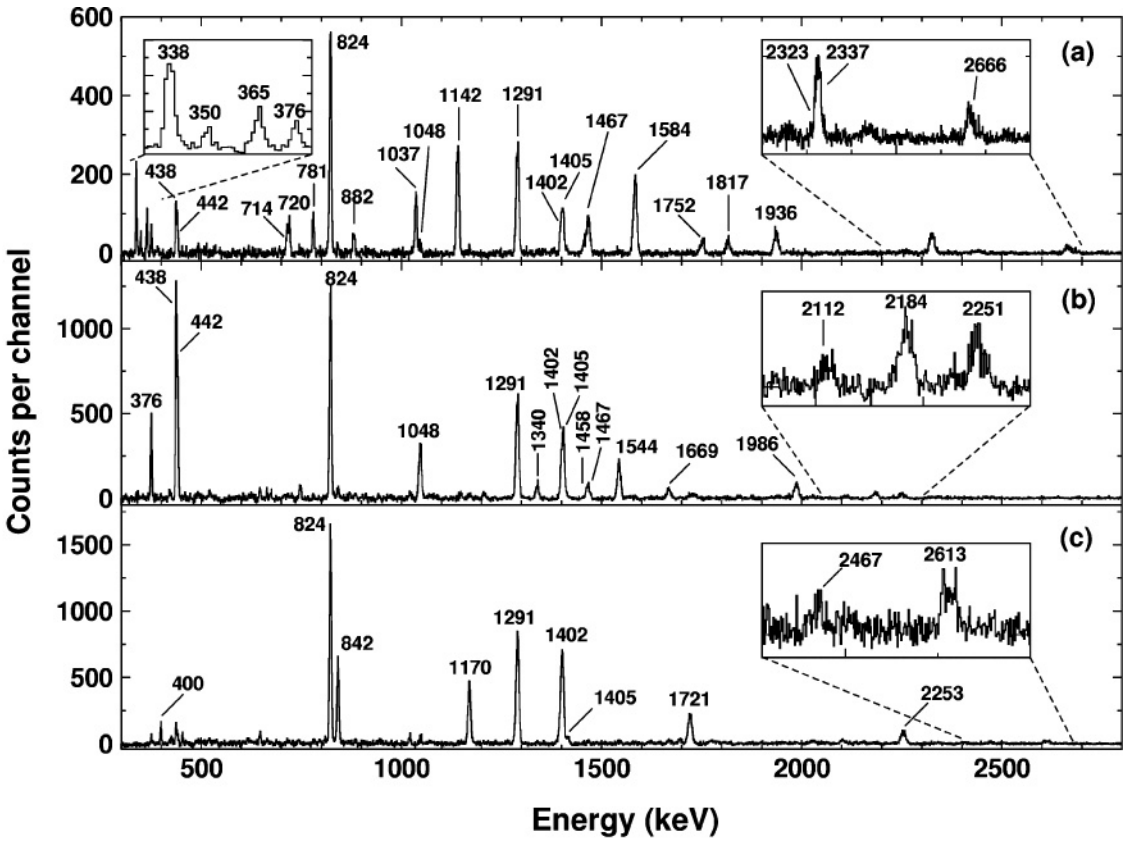

FIG. 6. Representative coincidence γ-ray spectra gated by transitions in ^{60}Fe: (a) gates set at 1936, 2323, and 2666 keV; (b) gates set at 1048, 1544, 1986, and 2184 keV; (c) gates set at 842, 1170, and 1721 keV. Peaks corresponding to transitions in ^{60}Fe are labeled by energy in keV. Insets show regions of the spectra at increased scales.

path through the 250-, 1581-, and 1126-keV transitions. While the 250-keV transition has an angular distribution indicative of a stretched-dipole nature, both the 1126- and 1582-keV transitions are consistent with a stretched-quadrupole nature, although the 1582-keV line has insufficient intensity for the extraction of a statistically significant a_4 coefficient. The angular distribution of the 816-keV γ rays, however, is also indicative of a quadrupole nature. With the spin assignments fixed by the transitions previously discussed, this γ ray must facilitate a spin change of $\Delta J = 1$, an argument supported by the fact that the measured a_2 coefficient approaches the upper limit of that of a highly mixed $11/2 \rightarrow 9/2$ transition.

The 494-keV transition that feeds the state at 1023 keV has a dipole angular distribution. This is consistent with the assignment of $J^\pi = 9/2^+$ at 1517 keV made by McLean *et al.* [28] using the ^{58}Fe$(d, p)^{59}$Fe and ^{57}Fe$(t, p)^{59}$Fe reactions. It is the assignment of positive parity which is the important input here from transfer studies, but such experiments also confirm spin-parities of other levels; the assignments of spin-parities $3/2^-$, $5/2^-$, and $7/2^-$ to the states at 0, 473, and 1023 keV, respectively, are consistent with those presented in Ref. [28]. The 795-, 1426-, and 1804-keV transitions all have angular distributions indicative of a stretched-quadrupole nature, thus extending the spin-parity assignments of the band to $21/2^+$ at 5542 keV (in the previous fusion-evaporation study of ^{59}Fe [26], the state at 3738 keV was given a lower limit of $J = 15/2$). The 2129-, 2532-, and 2712-keV transitions are assumed to continue the band of regular stretched-$E2$ transitions, hence the states at 7671, 10203, and 12915 keV have been given tentative assignments of $25/2^+$, $29/2^+$, and $33/2^+$, respectively.

Angular distributions could not be determined for the 1247-, 1420-, or 1240-keV transitions, because of contaminants. The level of statistics was too low for DCO ratios to provide an alternative means for deducing their multipolarities. However, the spin of the state at 3558 keV may be fixed via an alternative route. Both the 967- and 1789-keV γ rays have angular distributions characteristic of stretched-quadrupole transitions, leading to the assignments of $J^\pi = 13/2^+$ at 2483 keV and $17/2^+$ at 4273 keV. The 715-keV transition has a large negative a_2 coefficient and an a_4 coefficient consistent with zero, and as such the state at 3558 keV is assigned $J^\pi = 15/2^+$. Of the three transitions in the band feeding this state, the 2052-keV line is the only one for which an angular distribution could be measured, but as previously stated, this could only be accomplished by taking the distribution of the total sum of an unresolved doublet, and no statistically significant a_4 coefficient could be deduced. The large positive a_2 value, along with the fact that both transitions making up the doublet are of similar intensity, suggests that both are

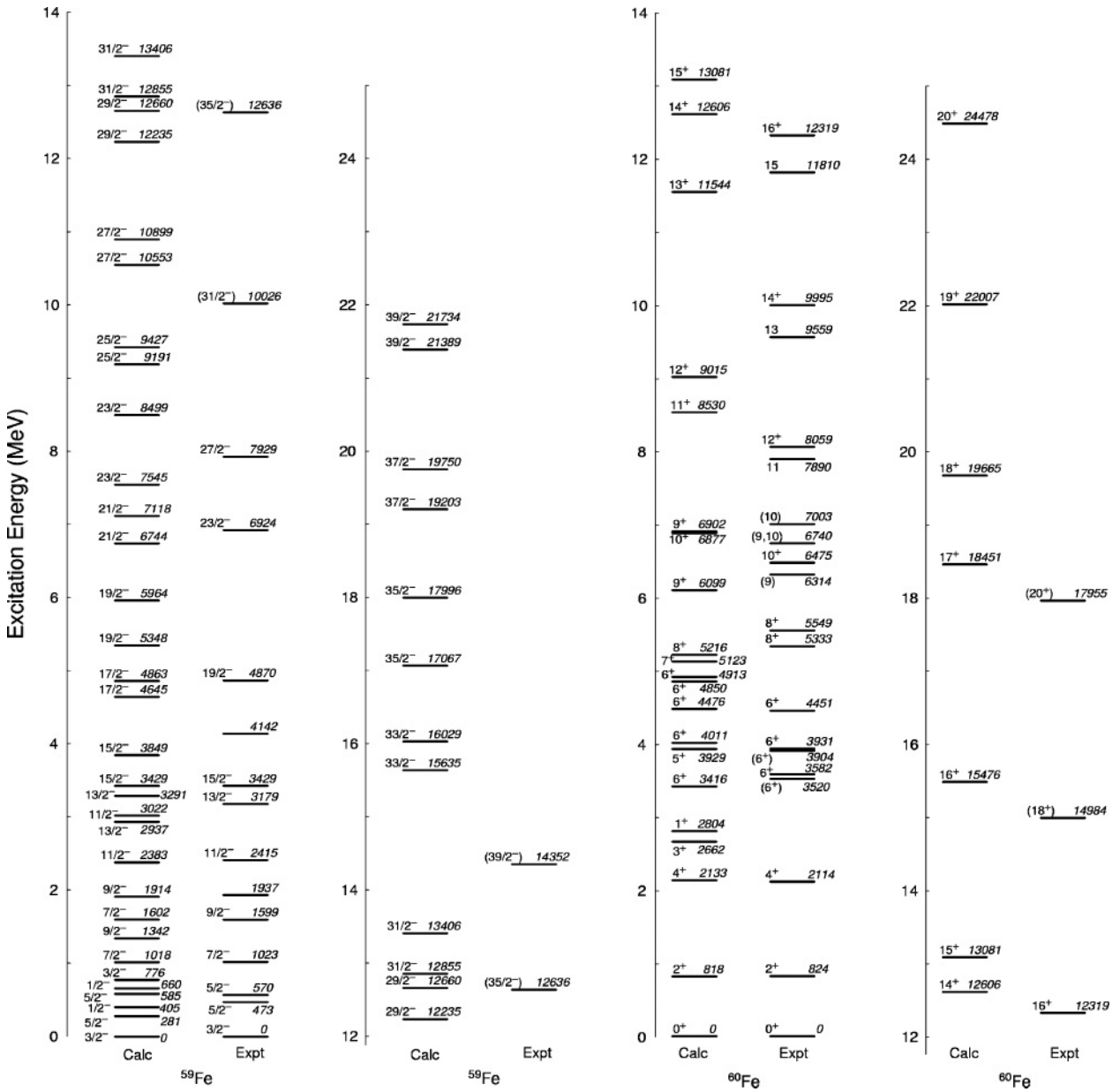

FIG. 7. Shell-model calculations for ^{59,60}Fe. The lowest two calculated states for each spin are shown, except in the case of the 6^+ states in ^{60}Fe, where five states are shown for comparison with the experimental levels.

of stretched-quadrupole character. Tentative assignments of $19/2^+$, $23/2^+$, and $27/2^+$ have been made to the states at 4978, 7030, and 9545 keV, respectively, based on the assumption that the 1420-, 2052-, and 2514-keV transitions make up a band of regular stretched-$E2$ transitions.

Parallel to the 1789-keV transition lie the 1221- and 568-keV lines. No angular distribution could be deduced for the 568-keV transition, as it is dominated by the much more intense 570-keV γ ray that feeds the ground state. Despite poor statistics, a positive a_2 coefficient was extracted for the 1221-keV transition, indicating it may have quadrupole character. The spin of the state at 3052 keV is, therefore, restricted to either 13/2 or 15/2. In either case, one of the two transitions appears to be highly mixed.

B. ^{60}Fe

The level scheme deduced for ^{60}Fe, presented in Fig. 5, has one strong sequence of transitions between positive-parity levels up to 20^+, and a pair of negative-parity sequences of similar intensity which are linked in their low-spin region. In general, spin assignments were made on the basis of fits to angular distribution data, of which representative examples are plotted in Fig. 3. The fitted a_2 and a_4 coefficients are listed in Table II.

Wilson *et al.* [29] were the first to identify and resolve the doublet formed from γ rays of energies 1402 and 1405 keV. This is confirmed in the current work, as are the majority of level and transition placements proposed in that work. No evidence has been found, however, for the 1475- and 1968-keV

TABLE II. Energies (in keV), spins and parities of excited states in ^{60}Fe. Measured transition energies E_γ and relative intensities I_γ (corrected for efficiency and internal conversion) of deexciting γ rays. The angular distribution coefficients, a_2 and a_4, and mixing ratios δ are also given where known. The a_2 and a_4 coefficients marked with superscripts were derived from the angular distribution of unresolved doublets. In each case the particular doublet is indicated by a different superscript.

Level energy	J^π	E_γ (keV)	I_γ	a_2	a_4
823.6(1)	2^+	823.6(1)	100(5)	+0.11(1)	−0.08(4)
2114.3(2)	4^+	1290.7(1)	92(3)	+0.23(1)	−0.08(2)
3515.9(2)	$5^{(-)}$	1401.7(1)	44.0(15)	−0.10(15)[a]	−0.05(2)[a]
3519.7(2)	(6^+)	1405.1(1)	16.1(8)	−0.10(15)[a]	−0.05(2)[a]
3581.8(2)	6^+	1467.4(1)	23.1(8)	+0.13(6)	−0.10(9)
3904.2(4)	(6^+)	1789.1(7)	0.7(2)		
3931.5(2)	6^+	349.5(1)	1.0(1)	+0.37(8)	
		1817.4(2)	6.4(3)	+0.51(8)	
3957.8(2)	$6^{(-)}$	375.9(1)	4.1(1)	+0.28(3)	
		437.9(1)	15.1(5)	+0.23(3)	−0.08(4)
		441.9(1)	7.1(2)	+0.39(4)	+0.17(6)
		1843(5)	0.2(1)		
4296.1(2)	$7^{(-)}$	338.2(1)	8.6(3)	−0.34(2)	
		364.5(1)	3.2(1)	−0.23(4)	
		714.4(1)	4.6(2)	−0.22(3)	
		780.6(10)	8.5(3)	+0.27(3)	−0.15(4)
4358.0(2)	$7^{(-)}$	399.9(1)	1.0(1)	+0.26(8)	
		426.4(4)	0.2(1)	−0.22(8)	
		453.7(2)	0.5(1)		
		842.3(1)	17.4(6)	+0.34(2)	−0.09(3)
4451.1(3)	6^+	2336.9(20)	2.9(2)	+0.40(10)	
5005.7(3)	$8^{(-)}$	647.7(2)	0.8(1)		
		1047.9(1)	17.1(5)	+0.31(2)	
5333.0(3)	$8^{(+)}$	882.0(2)	2.0(1)	+0.54(10)	
		1036.8(1)	9.2(3)	−0.38(3)	
		1751.6(2)	5.3(2)	+0.43(7)	
		1813.4(4)	1.9(1)		
5528.4(3)	$9^{(-)}$	522.8(2)	0.7(1)		
		1170.4(1)	15.1(5)	+0.43(3)	−0.13(4)
		1232.3(6)	0.7(1)		
5549.2(6)	8^+	1967.4(4)	2.2(2)	+0.18(10)	
5754.2(3)	$9^{(-)}$	748.5(1)	1.8(1)	−0.23(7)	
		1458.1(1)	10.1(3)	+0.73(5)	−0.12(7)
6314.3(6)	9	765.1(2)	0.9(1)	−0.34(10)	
6474.9(3)	10^+	720.3(3)	2.3(1)	−1.40(13)	
		1141.9(1)	18.0(6)	+0.37(2)	
6549.7(3)	$10^{(-)}$	1021.2(15)	0.2(1)		
		1544.0(1)	10.4(3)	+0.39(4)	−0.09(5)
6578.3(3)		824.0(1)	4.6(2)		
6739.7(5)	(9, 10)	1734.0(5)	0.9(1)		
6944.0(6)	10	1415.6(4)	1.3(1)	−0.45(6)[b]	
7003.0(7)	10	688.7(3)	0.4(1)	−0.44(14)	
7242.8(4)		664.5(1)	1.2(1)		
7249.8(3)	$11^{(-)}$	1721.3(1)	10.3(3)	+0.38(5)	−0.09(5)
7631.4(5)	$11^{(-)}$	1877.2(3)	2.6(1)	+0.55(14)	−0.37(19)
7664.6(4)		421.8(1)	1.2(1)		
7890.0(3)	11	1150.3(3)	0.9(1)		
		1340.3(1)	2.0(1)	−0.37(8)	
		1415.1(10)	1.5(1)	−0.45(6)[b]	
8059.1(3)	12^+	1584.2(1)	15.8(5)	+0.37(3)	−0.17(3)
8536.1(4)	$12^{(-)}$	1986.4(2)	3.2(1)	+0.36(8)	
8919.9(7)		1255.3(4)	0.4(1)		
8974.0(9)		2030.0(5)	1.1(1)		

TABLE II. *(Continued.)*

Level energy	J^π	E_γ (keV)	I_γ	a_2	a_4
9502.9(5)	(13^-)	2253.1(3)	3.3(2)	+0.35(5)[c]	−0.17(7)[c]
9559.0(3)	13	1499.9(2)	1.8(1)		
		1669.0(2)	3.5(1)	+0.46(6)	−0.15(8)
9995.4(4)	14^+	1936.3(1)	10.2(3)	+0.36(3)	−0.14(4)
10670.0(18)		1696.0(11)	0.4(1)		
10720.4(10)	(14^-)	2184.4(7)	0.9(1)		
11810.0(8)	15	2251.0(5)	1.9(1)	+0.35(5)[c]	−0.17(7)[c]
12115.8(15)	(15^-)	2612.9(10)	0.9(1)		
12318.5(21)	(16^+)	2323.1(15)	3.8(2)	+0.48(7)	−0.10(9)
12832.6(23)	(16^-)	2112.1(15)	0.4(1)		
14583.0(20)	(17^-)	2467.2(10)	0.2(1)		
14984.1(23)	(18^+)	2665.6(7)	1.3(1)		
17955(5)	(20^+)	2971(3)	0.3(1)		

transitions feeding the 2_1^+ state at 824 keV, nor for the 677-keV γ ray feeding the 4_1^+ level at 2114 keV, and hence the nonyrast 2^+ and 4^+ states placed at 2299 and 2792 keV, respectively, in Ref. [29] have been omitted from the new level scheme. Reference [29] used deep-inelastic collisions to populate states in ^{60}Fe, and differences in reaction mechanism may account for the nonobservation of levels in the current work.

As can be seen in Fig. 5, the current ^{60}Fe level scheme consists of three bands that appear quasirotational and extend to tentative spins of 20, 16, and 17$\hbar$. The positive-parity band exhibits a structural change at the 8^+ state, where there are sudden discontinuities in both the energy sequence and intensities of the transitions. A representative γ-ray spectrum formed by gating on transitions in this band is shown in Fig. 6(a). The two bands tentatively assigned negative parity are linked at lower spin by several weak transitions, possibly indicating that they are signature partners. The transitions in these bands can be seen in the representative spectra of Figs. 6(b) and 6(c). Aside from these bands, the rest of the level scheme is made up of a great many irregular transitions, from which little structural interpretation can be made.

The angular distributions measured for the 824-, 1291-, 1467-, 1752-, 1142-, 1584-, 1936-, and 2323-keV γ rays indicate these are all stretched-quadrupole transitions, thus securing the spin-parity assignments to the levels in the ground-state band from 0^+ through to 16^+ at 12319 keV. The two transitions above this state are assumed to continue the regular sequence of stretched-$E2$ transitions, leading to tentative assignments of 18^+ and 20^+ at 14984 and 17955 keV, respectively.

To the left of the ground-state band in Fig. 5, the 1967-keV transition has an angular distribution with no statistically significant a_4 coefficient, but the positive a_2 coefficient [+0.18(10)] suggests it has quadrupole character. In addition, yrast-feeding arguments suggest the 5549-keV level would have a spin greater than 7$\hbar$, and it is, therefore, assigned $J^\pi = 8^+$. The large, negative a_2 coefficients measured for the 765- and 689-keV transitions indicate a stretched-dipole character, leading to tentative spin assignments of 9 and 10$\hbar$ for the states at 6314 and 7003 keV.

The yrast 8_1^+ state at 5333 keV decays via several routes. Parallel to the 1752- and 1467-keV transitions between states with assignments $8_1^+ \rightarrow 6_1^+ \rightarrow 4_1^+$, is a decay path consisting of an 882- and a 2337-keV line. The large positive a_2 values of both these transitions agree with the assignment of $J^\pi = 6^+$ to the level at 4451 keV, although statistically significant a_4 values could not be deduced. A second path goes via a state at 3520 keV. This is tentatively assigned as $J^\pi = 6^+$ on the basis of yrast feeding arguments, as the 1813-keV transition is too weak to give a consistent angular distribution and the 1405-keV γ ray is an unresolvable doublet with the 1402-keV line. The angular distribution of this doublet has an uncharacteristic shape, which may be due to one transition being a dipole and the other a quadrupole. This complicates the assignments of both the tentative 6^+ state at 3520 keV and the level at 3516 keV, which decays via the 1402-keV γ ray. To assign a spin to the latter state, alternative decay paths must be examined. The path with the highest branching ratio out of the 5333-keV yrast 8^+ state has a 1037-keV transition with a stretched-dipole character, leading to a spin-7 level at 4296 keV (the parity of this state will be discussed later). This spin is supported by the dipole nature of the 714-keV line, decaying to the yrast 6^+ state at 3582 keV. In addition, the 4296-keV state itself decays by three other transitions with energies of 365, 338, and 781 keV. The 365- and 338-keV transitions have stretched-dipole angular distributions, and spin assignments of 6$\hbar$ are proposed for the states at 3958 and 3931 keV. The 781-keV transition, however, has a stretched-quadrupole distribution, indicating the state at 3516 keV must have a spin of 5$\hbar$.

Above the state at 3516 keV is another band of regular stretched-$E2$ transitions; the 842-, 1170-, 1721-, and 2253-keV γ rays take the spin assignments up to 13$\hbar$. The angular distribution of the 2253-keV transition is taken from the sum of the unresolved doublet with the 2251-keV transition, which has an overall distribution for the two equally intense transitions indicative of a quadrupole nature. As such, the $J = 13$ assignment at 9503 keV is tentative. The states at 12116 and 14583 keV are tentatively assigned spins of 15 and 17$\hbar$, based on the assumption that the regular band

of stretched-$E2$ transitions continues with those of 2613 and 2467 keV.

The parity of the band based on the spin-5 state at 3516 keV has been tentatively given as negative, based on supporting, but not definitive, model-dependent arguments. Shell-model calculations (discussed in detail later) place the lowest 5^+ state at 3929 keV, 413 keV above the experimental state in question, whereas other yrast positive-parity states in this spin regime are well reproduced. The $2_1^+, 4_1^+, 6_1^+$, and 8_1^+ experimental states, for example, lie within 6, 19, 166, and 117 keV of their respective theoretical counterparts. This suggests that the level at 3516 keV involves excitations beyond the fp space. Indeed, the fact that the band extends to spin 17 is supportive of this, as the maximum spin for a $\pi f_{7/2}^6 \nu(f_{5/2}p_{3/2}p_{1/2})^6$ configuration is 12^+. Involvement of the $g_{9/2}$ orbital increases the maximum spin; a $\pi f_{7/2}^6 \nu g_{9/2}(f_{5/2}p_{3/2}p_{1/2})^5$ configuration would generate $17\hbar$, but with negative parity, in contrast to the states generated in an fp space. It is therefore likely that the spin-5 state has negative parity and that the regular sequence above is a quasirotational structure up to a terminating spin of 17^- at 14.6 MeV. Two previous studies of ^{60}Fe are available for comparison at this point, both agreeing with spin assignments, but without measurements sensitive to parity changes. Reference [29] gives a tentative assignment of 5^+ to the state at 3516 keV but offers no arguments to support this. More recently, Hoteling *et al.* [30] studied ^{60}Fe via deep-inelastic reactions; their measurement of separate angular correlations for the 1402- and 1405-keV transitions confirms the spin assignments of 5 and $6\hbar$, at 3516 and 3520 keV, reported here.

Based on the tentative assignment of negative parity to the band above, the state at 4296 keV is given the same parity, by virtue of its connection to the 3516-keV state by the 781-keV γ ray of $E2$ character. The quadrupole angular distributions of the 1458- and 1877-keV lines lead to spin assignments of 9 and $11\hbar$, with the same parity as the lower levels in the sequence, for the states at 5754 and 7631 keV, respectively.

As already discussed, the levels at 3931 and 3958 keV are both assigned spins of $6\hbar$. In the latter case, there is a *weak* 1843-keV transition which decays to the 4_1^+ state. Ordinarily it would be assumed that any observed quadrupole transition must have an $E2$ character. The measured branching ratios for the four transitions observed as depopulating the state at 3958 keV can be compared with those predicted by typical transition rates for nuclei in this mass region [31]. If the 1843-keV transition has an $E2$ character, it would be expected to have a reduced transition rate of the order of 10^{13}s^{-1}, comparable to the 376-, 438-, and 442-keV transitions, and the four transitions would be expected to be have similar branching ratios. To obtain the observed branching ratio of 0.75% requires the 1843-keV transition to have an $M2$ character, such that the reduced transition rate would be of the order of 10^{10}s^{-1}. Therefore, the spin-6 state at 3958 keV is tentatively assigned negative parity. In the case of the other $6\hbar$ state at 3931 keV, the $\Delta J = 2$ transition to the 4_1^+ state is strong and an $E2$ assignment is appropriate. The angular distributions of the 1048-, 1544-, and 1986-keV γ rays above the 6^- state indicate that these lines form another band of regular stretched-quadrupole transitions, extending to spin $12\hbar$. Above this, tentative assignments of 14 and $16\hbar$ are based on the assumption that the 2184- and 2112-keV transitions continue the sequence.

Several of the transitions depopulating the levels at 3931 and 3958 keV appear to be mixed. The 442-keV transition, for example, has an angular distribution indicative of a $\Delta J = 1$ mixed transition. From the fitted a_2 and a_4 coefficients, an $E2/M1$ mixing ratio of $\delta = 2.6(6)$ has been estimated, indicating a sizable quadrupole component. The 438-keV transition has an angular distribution that could be interpreted as being that of a stretched-quadrupole character. However, with such an assignment, no consistent spin-parity choices could be achieved in the low-lying level scheme; the same measured angular distributions can be reproduced by a mixed, $\Delta J = 0$, transition with $\delta = 0.9(1)$. The 350- and 376-keV lines have angular distributions indicative of mixed, $\Delta J = 0, 1$, transitions. In keeping with the spin assignments discussed above, both transitions are assumed to be $\Delta J = 0$, and their mixing ratios have been deduced to be very small or zero. The interband 400-keV transition has a similar distribution, consistent with the assignment implicit in the previous discussion of $\Delta J = 1$. The mixing ratio of this transition is estimated to be $\delta = 0.31(6)$. No angular distributions could be measured for the remaining three interband transitions above this 4358-keV state.

Finally, there remain the spins of several states in side structures. In determining the spin of the level at 3904 keV, no angular distribution could be determined for the 454- or 1789-keV transitions. However, for consistency with the spin assignments already made, one of these transitions is likely to have $\Delta J = 1$ and the other $\Delta J = 2$, leading to a spin of 5 or $6\hbar$ for the state at 3904 keV. Yrast-feeding arguments suggest a 6^+ assignment.

The state at 6944 keV is tentatively assigned a spin of $10\hbar$, based on the angular distribution for the total sum of the 1415- and 1416-keV doublet (see below). The two states above this level have no assignments made, because distributions could not be measured for the 2030- and 1696-keV γ rays.

The states at 6578, 7243, 7665, and 8920 keV have no spins or parities assigned; the 824-keV transition is swamped by the $2_1^+ \rightarrow 0_1^+$ intensity.

The level at 7890-keV is assigned a spin of $11\hbar$, based on the dipole angular distribution of the 1340-keV transition. The angular distribution of the parallel decay via a 1415-keV level is difficult, as it forms a doublet with a transition of 1416 keV. The measurement of quadrupole angular distributions for the 1669- and 2251-keV transitions fix the spins of the states at 9559 and 11810 keV as 13 and $15\hbar$. No anisotropy could be obtained for the 1500-keV transition to support this assignment. The ordering of the 1150- and 1734-keV γ rays is uncertain because their relative intensities are similar. The state shown at 6740 keV could therefore lie at 6156 keV and is restricted to spins of 9 or $10\hbar$.

IV. DISCUSSION

Shell-model calculations for ^{59,60}Fe were carried out employing the GXPF1A interaction in the full fp model

space [8]; therefore, only the negative-parity experimental states in ^{59}Fe and positive-parity states in ^{60}Fe may be compared to the results of these calculations. In the case of both isotopes discussed here, however, this is particularly useful, as both systems have bands of natural-parity states extending to high energy and spin. Plots comparing shell-model and experimental levels for both isotopes are shown in Fig. 7

A. Shell-model calculations for ^{59}Fe

Agreement between near-yrast experimental negative-parity states and shell-model results is generally excellent up to the $15/2^-_1$ level. For example, the 570-, 1023-, 2415-, and 3429-keV experimental states are within 15, 5, 32, and <1 keV, respectively, of their theoretical counterparts, indicating a good description within the fp shell. In addition, the observed $13/2^-_2$ level at 3179 keV may correspond to the shell-model $13/2^-$ state at 3291 keV, as there is almost no $M1$ branch from $15/2^-_1$ to $13/2^-_1$ predicted in the shell model, in accord with the deduced experimental level scheme. A few irregularities appear between calculated and experimental states in this low-energy regime, most notably the 473-keV $5/2^-$ state, which lies 192 keV above the lowest predicted $5/2^-$ level, and the 1599-keV $9/2^-$ state, which lies 257 keV above and 315 keV below the two nearest $9/2^-$ levels resulting from the shell-model calculations. The fact that these experimental levels are considerably closer to theoretical states of different spins (namely, the $1/2^-$ state at 405 keV and the $7/2^-$ state at 1602 keV) may raise questions about the validity of the experimental spin-parity assignments. This point seems all the more pertinent given that the majority of low-lying experimental states lie so close to the predicted levels of matching spin-parity. However, the experimental assignments are rather firm. In the current data, angular distributions for the 473- and 1126-keV transitions appear to leave little question as to the assignments proposed in Fig. 2. Furthermore, spins of 1/2 and 7/2 at 473 and 1599 keV, respectively, would force the spin of the state at 3179 keV to be 11/2, thus being inconsistent with the angular distribution measured for the 250-keV transition. The $5/2^-$ level has also been populated using a variety of other methods including β decay, light-ion transfer, thermal-neutron capture, light-ion fusion-evaporation, and two-neutron transfer, as summarized in Ref. [32]. In (d, p) reactions it has been found to carry a significant fraction of the $1f_{5/2}$ strength with a spectroscopic factor of $(2J+1)S = 2.10$ quoted in Ref. [28], but clearly it has other strong admixtures of more complex configurations in its wave function. The $9/2^-$ state has not been populated in previous work.

Above the $15/2^-$ state at 3.4 MeV, correspondence between experiment and shell-model predictions is lost. The excitation energies for the yrast $19/2^-$ and $23/2^-$ states are predicted too high by about 0.5 MeV in the shell model. For the predicted yrast shell-model states, a sizable branch of $M1$ decay from $23/2^-$ to $21/2^-$ is expected, which is missing in the experimental data.

There is no obvious shell-model counterpart for the experimental $27/2^-$ level at 7929 keV in the same energy regime; to construct a $27/2^-$ state in the fp model space, the $N = 28$ core must be broken, placing the predicted state some 3 MeV above the yrast experimental $23/2^-$ level and much higher in excitation than the observed $27/2^-$ state.

The depression of experimental levels compared to fp-shell states is increasingly obvious at high spin. Above $27/2^-$ in the negative-parity band of ^{59}Fe, the experimental levels at 10026, 12636, and 14352 keV lie 2829, 4431, and 7037 keV *below* the lowest theoretical states of corresponding spin. The appearance of states much lower than fp-shell predictions suggests the influence of configurations beyond the model space. The extension of the band to spin 39/2, albeit tentative, supports this. Although technically possible, excitations in the full fp model space seem an unlikely explanation for such high-spin states at the observed energies; the $N = 28$ shell gap is estimated to be around 2 MeV in these nuclei [1]. With a minimum of three cross-shell excitations required to form a state of spin 39/2, the energy cost of doing so would be great. An alternative for constructing a spin-parity of $39/2^-$ is the promotion of two neutrons to the $g_{9/2}$ orbital. A $\pi f_{7/2}\,\nu g^2_{9/2}(f_{5/2}p_{3/2}p_{1/2})^3$ configuration has a maximum spin of 39/2 and is, therefore, consistent with termination in this case.

It is interesting to note that the negative-parity sequence above the $11/2^-$ state at 2.4 MeV shows increasing γ-ray energies up to $23/2^-$, followed by a sudden fall. This is suggestive of a structural change from predominantly $f_{5/2}p_{3/2}p_{1/2}$ configurations to those involving a pair of $g_{9/2}$ neutrons ($\nu g^2_{9/2}$). Another disruption of the sequence occurs at $35/2 \rightarrow 39/2$, possibly indicating the onset of termination of the latter configuration. Such interpretations are somewhat speculative since there are small numbers of transitions and the regularity of the sequences between configuration changes is not well established. In addition, parity assignments at the top of the sequence remain tentative.

As the shell-model calculations are based on the full fp model space, they cannot be used to assess the experimentally observed positive-parity states in Fig. 2. The band based on the $9/2^+$ state at 1517 keV appears quasirotational in character and is most likely based on the promotion of the odd neutron to the $g_{9/2}$ orbital. This is confirmed by the large spectroscopic factor, $2(J+1)S = 5.1$, obtained for the $\ell = 4$ transition to this state reported previously in (d, p) reactions [28]. The maximum spin of such a configuration corresponds to that (tentatively) assigned to the highest-energy state of the band: 33/2. The excitation energy of this single-neutron excitation to $g_{9/2}$ is not inconsistent with the expectation of $g^2_{9/2}$ contributions to the high-spin portion of the negative-parity band.

B. Shell-model calculations for ^{60}Fe

Agreement between experimental data and shell-model results is good for the yrast 2^+ and 4^+ states, which lie within 6 and 19 keV of the calculated states. The experimental 6^+ (3582 keV), 8^+ (5549 keV), tentative spin-9 (6314 keV), and 10^+ (7003 keV) states are likely to correspond to calculated yrast 6^+ (3416 keV), 8^+ (5216 keV), 9^+ (6099 keV), 10^+ (6877 keV) states, respectively, according to the excitation

energies and transition properties. There are five experimental 6^+ levels (two tentative) between the excitation energies of 3520 and 4451 keV. The five lowest 6^+ states generated in the shell-model calculations are given in Fig. 7, but it is difficult to see correspondence between all of these and the experimental data.

There is little or no correspondence between the experimental data and shell-model results for most other states. For example, the regular band on top of the experimental 8^+ state at 5333 keV is difficult to find in the shell model. The yrast band predicted by the shell model shows rather irregular γ-ray energies and much smaller moments of inertia and is therefore highly nonyrast in comparison with the experimental data. It seems likely, therefore, that the origin of this band may be from outside the fp space. However, the positive parity of this band, inferred from the measurement of quadrupole angular distributions up to $J = 16$, would require the involvement of an even number of $g_{9/2}$ neutrons. This suggestion is supported by the tentative assignment of $J = 20^+$ to the highest state in the band, which corresponds to the maximum spin for a $\pi f_{7/2}^6\, \nu g_{9/2}^2 (f_{5/2} p_{3/2} p_{1/2})^4$ configuration. Other major structures in ^{60}Fe are thought to be of negative parity and, therefore, explicitly beyond the fp model space.

In the Cr isotopes, fairly reasonable correspondence was found between observed levels and states calculated in the fp space for $N \leqslant 34$. However, the observed levels were restricted to spin values less than $10\hbar$ and excitation energies below $\sim$5 MeV. The current observations have highlighted issues with fp-shell configurations in the higher-spin, higher-excitation regime, where it is clear that $g_{9/2}$ excitations play a significant role.

C. Collective structures

The discussion above, together with other recent observations, indicates that the $\nu g_{9/2}$ excitations are a ubiquitous feature of high-spin structures across neutron-rich fp-shell nuclei. The deformation-driving nature of this orbital leads to the development of quasirotational structures in Cr nuclei [12–14], which can be understood to some extent using total Routhian surface (TRS) calculations. The shortcomings of such calculations are related to the softness in the calculated shapes because of the transitional nature of the nuclei in question.

Similar regular sequences of γ-ray transitions are now seen at high spin in Fe isotopes. The extracted aligned angular momenta also exhibit smooth regular features, illustrated in Fig. 8, which suggest collective behavior in the higher-spin regime. This figure also shows the aligned angular momenta I_x for high-spin sequences in neutron-rich Cr isotopes, where different isotopes generally also exhibit similar slopes in the variation of I_x with frequency. ^{57}Cr exhibits an upbend which has been associated with the alignment of $f_{7/2}$ protons by comparison with TRS calculations. The latter give a reasonable description of the bands in this case [12].

The alignments in the Fe isotopes have a common gradient, but it is not quite as steep as in the Cr case. This is possibly related to changes in deformation, although it may also be due to changes in the configurations involved. The negative-parity sequences in ^{60}Fe show upbends similar to that seen in ^{57}Cr, at comparable or slightly higher frequencies. This may be due to the Fermi surface being farther from the $\Omega = 1/2$ state in the former case. The other high-spin bands do not exhibit clear evidence of upbends. In particular, the ground-state band in ^{60}Fe shows a smooth trend up to the highest rotational frequencies observed. It is possible that the excitation of two $g_{9/2}$ neutrons in this configuration produces higher deformation, pushing the upbend to higher spins. We note that the fact that the I_x values for this band are larger than those of all other bands is consistent with the interpretation of this being the sole excitation involving two aligned $g_{9/2}$ neutrons. The bands in ^{59}Fe are observed to frequencies comparable to those of the observed upbends, but it is possible that these sequences have not been extended high enough in the present work; there is some indication that the

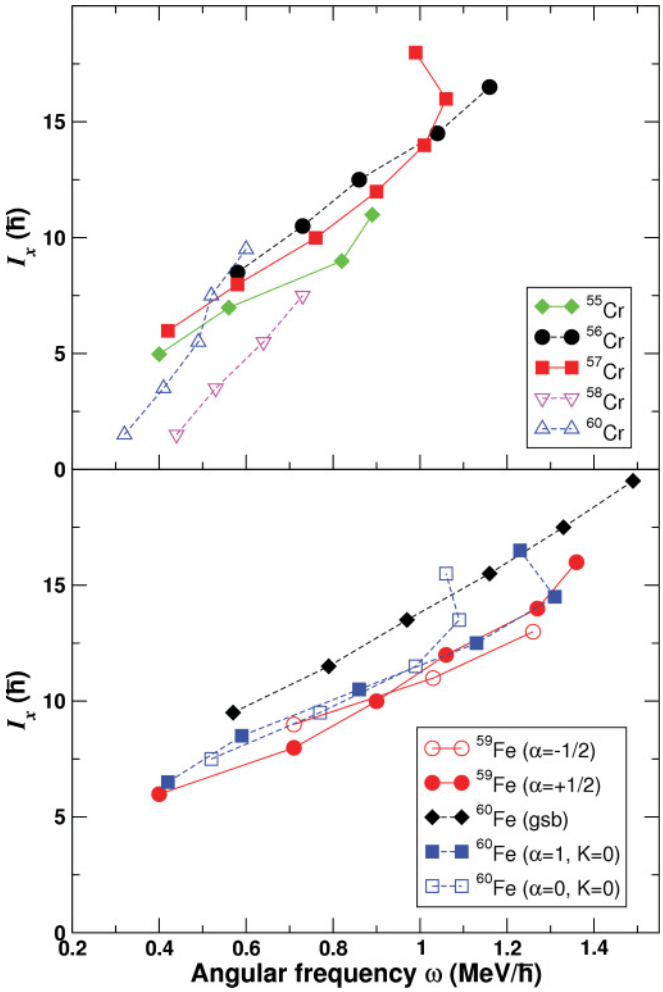

FIG. 8. (Color online) Experimental aligned angular momenta, I_x, as a function of rotational frequency ω. Data in the top panel are taken from Refs. [4,12,14]; data in the bottom panel are taken from the current work. All bands are assumed to have a negligible K value; in the case of the ^{60}Fe $\alpha = 0, 1$ bands, a high K value shifts the data points down in angular frequency by around 0.1 MeV/$\hbar$. The ground-state band points correspond to the yrast sequence starting at spin 8.

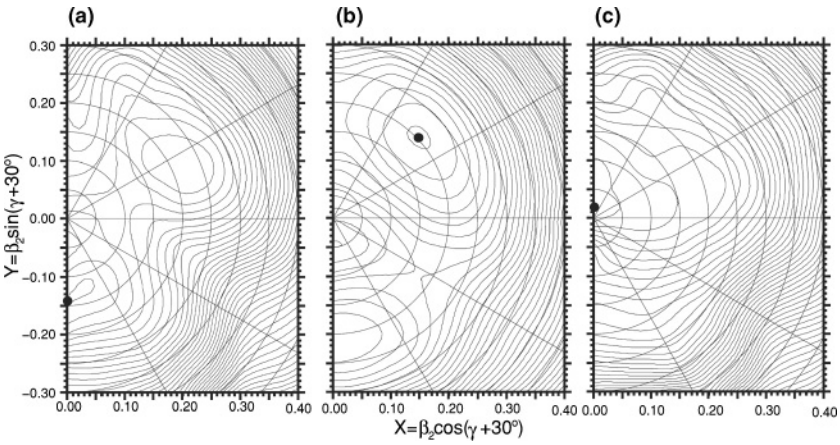

FIG. 9. Potential-energy surfaces for (a) the negative-parity band in ^{59}Fe, with angular frequency $\omega = 1.0$ MeV/$\hbar$, (b) the positive-parity band based on the $g_{9/2}$ state at 1517 keV, with $\omega = 0.2$ MeV/$\hbar$, and (c) same as (b) but with $\omega = 1.0$ MeV/$\hbar$. All plots are taken from the TRS calculations described in the text. Contours are shown at 200-keV intervals; location of the absolute minimum is indicated by a dot in each panel.

beginning of an upbend is seen in the $\alpha = +1/2$ sequence in ^{59}Fe.

In an attempt to clarify the physical situation, TRS calculations [33] were performed with the nonaxial deformed Woods-Saxon potential and the Universal parameter set of Ref. [34]. Figure 9(a) presents the results of these calculations for the yrast negative-parity band in ^{59}Fe at an angular frequency of 1.0 MeV/$\hbar$. A minimum in the energy surface is associated with a prolate shape ($\gamma \sim 0^\circ$) with a quadrupole deformation $\beta_2 \sim 0.2$. At this rotational frequency and deformation, both $\nu g_{9/2}$ and $\pi f_{7/2}$ quasiparticle pairs have aligned. With the neutron Fermi surface lying low in the $g_{9/2}$ shell, aligning $g_{9/2}$ quasiparticles will polarize the nuclear shape toward $+30^\circ$. Conversely, the proton Fermi surface lies near the top of the $f_{7/2}$ shell, and aligning $f_{7/2}$ quasiparticle pairs will polarize the nuclear shape toward -30° in γ. The near axial symmetric shape calculated in Fig. 9(a) suggests that the opposite polarizing effects of aligned neutrons and protons cancel each other out.

The results for the yrast positive-parity sequence are given in Figs. 9(b) and 9(c), at angular frequencies of 0.2 and 1.0 MeV/$\hbar$, respectively. The triaxial minimum at $\beta_2 \sim 0.2$ and $\gamma \sim 15^\circ$ in Fig. 9(b) demonstrates the shape-driving effects of a single $g_{9/2}$ quasineutron toward positive γ values which can be contrasted with Fig. 9(a). The total Routhian surface in Fig. 9(c) is heavily influenced by the $\pi f_{7/2}$ alignment which takes place around $\hbar\omega = 0.9$–1.0 MeV. With only one $g_{9/2}$ orbital occupied, the polarizing effects of the aligned $f_{7/2}$ quasiproton pair drive the equilibrium deformation to $\gamma \sim -20^\circ$ and $\beta_2 \sim 0.17$. In contrast to Fig. 9(a), the single $g_{9/2}$ quasiparticle is unable to compensate for the polarizing influence of the $f_{7/2}$ protons. As a consequence, the surface in Fig. 9(c) is suggesting a triaxial deformation, but it is quite shallow and soft in both the γ and β_2 degrees of freedom.

All three total Routhian surfaces in Fig. 9 demonstrate that the shape of a particular configuration is greatly influenced by the aligned quasiparticles it contains and highlight a situation where the underlying cores are soft with respect to deformation. This is not unexpected in systems exhibiting both spherical and deformed structures. Similar surfaces are found for the ground-state band in ^{60}Fe. Such soft, ill-defined shapes present challenges for a definitive interpretation of the high-spin sequences. Accurate calculations are difficult due also to the expectation of a strong influence from vibrational effects, not included in the current models.

It is, hence, difficult to substantiate the remarks made above in relation to alignment systematics using current theoretical models. To illustrate this, we return to Fig. 8. The TRS calculations would predict an $f_{7/2}$ proton alignment to occur for all bands plotted in the lower panel of Fig. 8 between 0.8 and 1.0 MeV. Only the two negative-parity bands in ^{60}Fe indicate a possible alignment at 1.1 and 1.3 MeV/$\hbar$ in the $\alpha = 0$ and $\alpha = 1$ sequences, respectively. While this behavior could be attributed to the alignment of $f_{7/2}$ quasiprotons, the calculations also indicate that secondary $g_{9/2}$ alignments (i.e., so-called BC and AD crossings) should take place in the same 1.1 MeV/$\hbar$ frequency range. The latter possibility is, in a way, more consistent with the experimental data because (i) the upbend in the two bands occurs at different rotational frequencies and (ii) no such crossing is observed in the ground-state band of ^{60}Fe where the $\nu(g_{9/2})^2$ configuration blocks the secondary crossings. As a consequence, it would then follow that the predicted proton $f_{7/2}$ alignment is completely absent in the data, or at least it is not visible in the frequency domain under investigation. Clearly, more sophisticated calculations are required to make further progress in understanding the high-spin sequences.

V. CONCLUSIONS

Yrast and near-yrast states in ^{59,60}Fe have been studied with the Gammasphere array using the heavy-ion fusion-evaporation of ^{48}Ca projectiles with enriched ^{13,14}C targets. Extended level schemes for both nuclei are now available. In both cases, shell-model calculations using the GXPF1A interaction in the full fp model space satisfactorily reproduce the low-lying, natural-parity states. However, both nuclei also exhibit high-spin structures that deviate from the calculations, indicating the intrusion of the $g_{9/2}$ orbital, as seen in other neutron-rich fp-shell nuclei.

In ^{59}Fe, a negative-parity band extends to high spin, which may correspond to the excitation of two $g_{9/2}$ neutrons, although evidence for this is only tentative. The positive-parity band

appears to be based on a single $g_{9/2}$ neutron excitation. TRS calculations indicate a very soft core, and the equilibrium shapes extracted from the model are greatly influenced by the number and parentage of the aligned quasiparticles. The comparison of data in these neutron-rich systems with current shell-model calculations indicates that there is strong motivation for extending the interactions to include the neutron $g_{9/2}$ orbital in a general fashion.

ACKNOWLEDGMENTS

This work was supported by the U.K. Science and Technology Facilities Council, the U.S. Department of Energy, Office of Nuclear Physics, under Contract Nos. DE-AC02-06CH11357 and DE-FG02-94ER40848, and the U.S. National Science Foundation under Grant PHY-0139950. The authors would also like to thank M. Freer at Birmingham University for the use of the ^{14}C target.

[1] M. Honma, T. Otsuka, B. A. Brown, and T. Mizusaki, Phys. Rev. C **65**, 061301(R) (2002).
[2] R. V. F. Janssens, B. Fornal, P. F. Mantica, B. A. Brown, R. Broda, P. Bhattacharyya, M. P. Carpenter, M. Cinausero, P. J. Daly, A. D. Davies *et al.*, Phys. Lett. **B546**, 55 (2002).
[3] D.-C. Dinca, R. V. F. Janssens, A. Gade, D. Bazin, R. Broda, B. A. Brown, C. M. Campbell, M. P. Carpenter, P. Chowdhury, J. M. Cook *et al.*, Phys. Rev. C **71**, 041302(R) (2005).
[4] D. E. Appelbe, C. J. Barton, M. H. Muikku, J. Simpson, D. D. Warner, C. W. Beausang, M. A. Caprio, J. R. Cooper, J. R. Novak, N. V. Zamfir *et al.*, Phys. Rev. C **67**, 034309 (2003).
[5] P. F. Mantica, A. C. Morton, B. A. Brown, A. D. Davies, T. Glasmacher, D. E. Groh, S. N. Liddick, D. J. Morrissey, W. F. Mueller, H. Schatz *et al.*, Phys. Rev. C **67**, 014311 (2003).
[6] A. M. Nathan, J. W. Olness, E. K. Warburton, and J. B. McGrory, Phys. Rev. C **17**, 1008 (1978).
[7] A. Gade, R. V. F. Janssens, D. Bazin, R. Broda, B. A. Brown, C. M. Campbell, M. P. Carpenter, J. M. Cook, A. N. Deacon, D.-C. Dinca *et al.*, Phys. Rev. C **74**, 021302(R) (2006).
[8] M. Honma, T. Otsuka, B. A. Brown, and T. Mizusaki, Eur. Phys. J. A **25**, s01, 499 (2005).
[9] B. Fornal, S. Zhu, R. V. F. Janssens, M. Honma, R. Broda, B. A. Brown, M. P. Carpenter, S. J. Freeman, N. Hammond, F. G. Kondev *et al.*, Phys. Rev. C **72**, 044315 (2005).
[10] A. Gade, R. V. F. Janssens, D. Bazin, B. A. Brown, C. M. Campbell, M. P. Carpenter, J. M. Cook, A. N. Deacon, D.-C. Dinca, S. J. Freeman *et al.*, Phys. Rev. C **74**, 047302 (2006).
[11] C. N. Davids, D. F. Geesaman, S. L. Tabor, M. J. Murphy, E. B. Norman, and R. C. Pardo, Phys. Rev. C **17**, 1815 (1978).
[12] A. N. Deacon, S. J. Freeman, R. V. F. Janssens, F. R. Xu, M. P. Carpenter, I. R. Calderin, P. Chowdhury, N. J. Hammond, T. Lauritsen, C. J. Lister *et al.*, Phys. Lett. **B622**, 151 (2005).
[13] S. J. Freeman, R. V. F. Janssens, B. A. Brown, M. P. Carpenter, S. M. Fischer, N. J. Hammond, M. Honma, T. Lauritsen, C. J. Lister, T. L. Khoo *et al.*, Phys. Rev. C **69**, 064301 (2004).
[14] S. Zhu, A. N. Deacon, S. J. Freeman, R. V. F. Janssens, B. Fornal, M. Honma, F. R. Xu, R. Broda, I. R. Calderin, M. P. Carpenter *et al.*, Phys. Rev. C **74**, 064315 (2006).
[15] O. Sorlin, C. Donzaud, F. Nowacki, J. C. Angélique, F. Azaiez, C. Bourgeois, V. Chiste, Z. Dlouhy, S. Grévy, D. Guillemaud-Mueller *et al.*, Eur. Phys. J. A **16**, 55 (2003).
[16] D. Steppenbeck *et al.* (to be submitted).
[17] N. Hoteling, W. B. Walters, R. V. F. Janssens, R. Broda, M. P. Carpenter, B. Fornal, A. A. Hecht, M. Hjorth-Jensen, W. Krolas, T. Lauritsen *et al.*, Phys. Rev. C **74**, 064313 (2006).
[18] R. Broda, J. Phys. G: Nucl. Part. Phys. **32**, R151 (2006).
[19] B. Fornal, Acta Phys. Pol. B **26**, 357 (1995).
[20] W. Królas, R. Broda, B. Fornal, T. Pawłat, H. Grawe, K. H. Maier, M. Schramm, and R. Schubart, Nucl. Phys. **A724**, 289 (2003).
[21] L. Corradi, A. M. Stefanini, C. J. Lin, S. Beghini, G. Montagnoli, F. Scarlassara, G. Pollarolo, and A. Winther, Phys. Rev. C **59**, 261 (1999).
[22] I.-Y. Lee, Nucl. Phys. **520**, 641c (1990).
[23] C. N. Davids, B. B. Back, K. Bindra, D. J. Henderson, W. Kutschera, T. Lauritsen, Y. Nagame, P. Sugathan, A. V. Ramayya, and W. B. Walters, Nucl. Instrum. Methods B **70**, 358 (1992).
[24] A. Gavron, Phys. Rev. C **21**, 230 (1980).
[25] H. J. Kim, Nucl. Data Sheets **17**, 485 (1976).
[26] E. K. Warburton, J. W. Olness, A. M. Nathan, J. J. Kolata, and J. B. McGrory, Phys. Rev. C **16**, 1027 (1977).
[27] R. Holzmann, I. Ahmad, R. V. F. Janssens, T. L. Khoo, D. C. Radford, M. W. Drigert, and U. Garg, Nucl. Instrum. Methods A **260**, 153 (1987).
[28] K. C. McClean, S. M. Polgliesh, S. S. Ipson, and G. Brown, Nucl. Phys. **A191**, 417 (1972).
[29] A. N. Wilson, C. W. Beausang, N. Amzal, D. E. Appelbe, S. Asztalos, P. A. Butler, R. M. Clark, P. Fallon, and A. O. Macchiavelli, Eur. Phys. J. A **9**, 183 (2000).
[30] N. Hoteling *et al.* (private communication).
[31] P. M. Endt and C. van der Leun, At. Data Nucl. Data Tables **13**, 67 (1974).
[32] C. M. Baglin, Nucl. Data Sheets **95**, 215 (2002).
[33] F. R. Xu, W. Satula, and R. Wyss, Nucl. Phys. **A669**, 119 (2000).
[34] W. Nazarewicz, J. Dudek, R. Bengtsson, T. Bengtsson, and I. Ragnarsson, Nucl. Phys. **435**, 397 (1985).